Journal of Molecular Liquids 233 (2017) 75–88

Contents lists available at ScienceDirect

Journal of Molecular Liquids

journal homepage: www.elsevier.com/locate/molliq

Application of graphene oxide modified with 8-hydroxyquinoline for the adsorption of Cr (VI) from wastewater: Optimization, kinetic, thermodynamic and equilibrium studies

Amir Sheikhmohammadi [a], Seyed Mohsen Mohseni [b], Rouhollah khodadadi [c], Mahdieh Sardar [d], Mehrnoosh Abtahi [d], Sakineh Mahdavi [e], Hassan Keramati [f], Zohreh Dahaghin [g], Soheila Rezaei [h], Mohammad Almasian [i], Maryam Sarkhosh [j,*], Majid Faraji [k], Shahram Nazari [l]

[a] Students Research Office, Department of Environmental Health Engineering, School of Health, Shahid Beheshti University of Medical Sciences, Tehran, Iran
[b] Department of Environmental Health Engineering, School of Health, Qom University of Medical Sciences, Qom, Iran
[c] Department of Environmental Health Engineering, School of Health, Ahvaz Jundishapur University of Medical Sciences, Ahvaz, Iran
[d] Department of Environmental Health Engineering, School of Health, Shahid Beheshti University of Medical Sciences, Tehran, Iran
[e] Occupational Health Engineering Department, School of Public Health, Lorestan University of Medical Sciences, Khorram Abad, Iran
[f] Department of environmental Health Engineering, School of Public Health, Semnan University of Medical Sciences, Semnan, Iran
[g] Young Researchers and Elite club, Central Tehran Branch, Islamic Azad university, Tehran, Iran
[h] Social Determinants of Health Research Center, Yasuj University of Medical Sciences, Yasuj, Iran
[i] Department of the English Language, School of Medicine, Lorestan University of Medical Sciences, Khorramabad, Iran
[j] Department of Environmental Health Engineering, School of Health, Mashhad University of Medical Sciences, Mashhad, Iran
[k] Research Center for Environmental Determinants of Health (RCEDH), Kermanshah University of Medical Sciences, Kermanshah, Iran
[l] Department of Environmental Health Engineering, School of Public Health, Iran University of Medical Sciences, Tehran, Iran

ARTICLE INFO

Article history:
Received 25 October 2016
Received in revised form 23 February 2017
Accepted 24 February 2017
Available online 1 March 2017

Keywords:
8-hydroxyquinoline-modified graphene oxide
Modeling
Optimization
Kinetic
Thermodynamic
Isotherm
Cr (VI)

ABSTRACT

In the present study, removal of Cr (VI) from aqueous solution was investigated by adsorption onto graphene oxide modified with 8-hydroxyquinoline (8-HQ- GO-Fe_3O_4). Graphen oxide (GO) sheets, magnetic GO -Fe_3O_4 nanocomposite and the 8-HQ - functionalized GO-Fe_3O_4 nanocomposite (8- HQ - GO-Fe_3O_4) were freshly synthesized and characterized by Scanning electron microscope (SEM) images, Fourier transform infrared (FTIR) spectroscopy, energy dispersive X-ray (EDAX) and thermogravimetric (TGA) analysis. The response surface methodology using R software was chosen to investigate the composition effect of input independent factors (pH, 8-HQ/GO dose, time and Cr (VI) concentration) and one dependent output response (removal efficiency). The lower *P*-value (1.33×10^{-15}), higher F-value (240.4), higher R^2 (multiple R-squared: 0.994, adjusted R-squared: 0.989) and insignificant lack of fit (0.38) indicate that reduced full second-order model has highly significant for adsorption of Cr (VI) by 8-HQ- GO-Fe_3O_4 and it also is represented satisfactory adjustment between model and experimental data. The predicted optimal conditions by model (to involve all parameters simultaneously) for the maximum removal efficiency (95.77%) were achieved (pH, 6.58; 8-HQ/GO dosage, 98.4 g L^{-1}; contact time, 178.4 min and Cr (VI) concentration, 1 mg L^{-1}). Based on reported results, a high correlation coefficient (R^2) was found for the Langmuir model compared with the Freundlich and the Temkin models that confirm the reasonably fit to the data. The maximum adsorption capacity calculated from the Langmuir was 11.9 mg g^{-1} at 308 K. The kinetics followed is pseudo second order in nature and the intraparticle diffusion was the dominating mechanism. The thermodynamic data revealed the endothermic nature, an increase in the degree of freedom of the adsorbed ions and spontaneous sorption for the adsorption process. Also the Ea value found to be 1.39 kJ mol^{-1} indicating chemical sorption.

1. Introduction

As one of the most serious environmental pollutants, chromium includes various oxidation states ranging from +6 to −2. However, it has been proven that only the +6 and +3 oxidation forms are stable in natural environments [1–3]. In an aquatic system, hexavalent chromium (Cr (VI)), such as chromate [CrO_4^{2-}, $HCrO_4^-$], is highly mobile, soluble reactive, can impact large-volume aquifers, and affects biological systems due to its strong oxidizing properties [4,5]. In contrast, the reduced form of chromium, Cr(III), is a required nutrient for the proper functioning of living organisms [6], it is less mobile in the environment, much less

* Corresponding author.
E-mail address: marya.sarkhosh@yahoo.com (M. Sarkhosh).

http://dx.doi.org/10.1016/j.molliq.2017.02.101
0167-7322/

toxic, and is not hazardous (compared with Cr (VI)) due to its low solubility) [4,7]. Hexavalent chromium, Cr (VI), is a common contaminant in soil and groundwater and is classified as a priority pollutant by the US Environmental Protection Agency (EPA) [8]. It is more toxic (about 500–1000 times) than Cr (III). The main causes for the release of significant quantities of Cr (VI) into the environment can be due to leakage, unsuitable storage and/or improper disposal practices from industrial processes such as metallurgical, pigments producing, electroplating, tanning, metal finishing processes, and chromium mining operations [9,10]. The Cr (VI) as a potential carcinogen to humans, animals, plants and microorganisms [4] can cause dermatitis, rhinitis, and even lung and nasopharyngeal cancers [6,9,11]. The EPA has recommended a maximum contaminant level (MCL) of 0.1 mg L^{-1} and 0.05 mg L^{-1} for Cr (VI) for inland surface and potable waters, respectively [7,10,12]. Therefore, the removal of Cr (VI) from water solutions before its release into the environmental is a critical issue. For this purpose, scientists have, in recent years, investigated several methods to eliminate or lessen the concentration of Cr (VI) and heavy metals [13], including adsorption onto solid adsorbents [14], reduction [15], electrochemical processes [16], biosorption on fungi and algae [17,18], membrane filtration [18], precipitation [19], ion exchange [20], carbonaceous nanofibers [21], a core–shell structure of polyaniline coated protonic titanate nanobelt composites [22], and other methods. Scientists are studying new and alternative technologies in order to develop efficient and cost-effective treatments for the removal of such pollutants [23,24]. In the field of wastewater remediation, adsorption approach has been widely utilized in the attenuation of metals in wastewater, due to its simplicity, high efficiency, and its ability to recycle both metal ions and solid adsorbents [18,25–29]. Graphene, a single-atom-thick and two-dimensional carbon nanomaterial (composed of a single layer of sp^2 network of carbon atoms [30], as the basic building block of all graphitic forms (carbon nanotubes, graphite, and fullerene C60) [31], has attracted a great deal of scientific interest in recent years. Graphene oxide (GO) is always obtained through the strong oxidation of graphite that contains different forms of oxygen atoms (epoxy, hydroxyl, and carboxyl groups) on its surface. The presence of these functional groups on the GO provides specific surface structures that make it possible for it to be used as an adequate adsorbent. Some researchers have reported the emerging application of GO as an effective adsorbent for the removal of ammonia [32], formaldehyde [33], Hg^{2+} [34], Cu^{2+} [35] and methyl blue [36]. Although, it should be noted potential toxicity and high mobility of GO in environment that can cause serious effect in livings such as accumulate in the lung, liver and spleen for long time. It may be because of not easily conversion of GO into harmless-end products or degradation to non-toxic small molecules, which tends to aggregate in living organisms with the van der Waals interactions between neighboring sheets in water. For determination its industrial applications and ecological impacts, the colloidal stability of GO in the aquatic solution should be assessed [37,38]. GO has been proven to exhibit great promise for potential applications in the environmental pollutant removal because of large amounts of oxygen-containing functional groups on its basal planes and edges [39]. However, the difficult separation of carbon materials from the final system result limits their potential application in adsorption. Recently, the flexibility and simplicity of use of magnetic materials in adsorption of pollutants has been demonstrated [40,41]. Therefore, the preparation of magnetic GO can be a convenient method, which can later be attracted by an external magnetic field as shown by several studies, such as the use of $MnFe_2O_4$/AC magnetic composite for the removal of tetracycline [42], g-Fe_2O_3/carbon hybrids for the removal of Cr (VI) [43], mesoporous Fe_2O_3@C encapsulates for the removal of As [44], and multiwall carbon nanotube/iron oxide magnetic composites for the removal of Ni (II) and Sr (II) [45]. The modification of GO is considered an important route for the enhancement of removal efficiency, selectivity, and sensitivity of heavy metals. The modification can be done via the formation of a chemical bond between the modifier species and GO surface, or physically through the adsorption of the modifier onto the GO surface [46]. There have been some well-known techniques to improve removal of pollutants from aqueous solution using GO. Yu et al. applied magnetite decorated graphene oxide for the highly efficient immobilization of Eu(III) from aqueous solution. They revealed the combination of the excellent adsorption capacity of GO and the magnetic properties of magnetite can be a promising candidate for the removal of Eu(III) and related radionuclides from aqueous solutions in nuclear waste management [29].

The 8-Hydroxyquinoline (8-HQ), also known as 8-quinolinol or oxine, is chemically immobilized on different solid supports such as chelating resin, bentonite, and silica nanoparticles to form various solid absorbents, where it has been shown to greatly enhance the removal of heavy metal ions from aqueous solutions [47–49]. 8-HQ is a kind of strong bidentate chelating agent [50,51] that contains an oxygen donor atom and a nitrogen donor atom (as two coordination atoms) which can be used as a modifying agent for various sorbents through the formation of a chelate ring [13,25,52]. In order to improve process efficiency, minimize operational costs and time, and take into account the most important factors, it is essential to use the optimization techniques in application of 8-HQ/GO on an industrial scale. The classical optimization method (changing one factor and fixing others) is not as precise and reliable as expected, because it does not depict the interactive effects of all the involved factors. Additionally, such studies require spending a long time and performing numerous tests [53–55]. There are good commercial software, such as Design-Expert [56], JMP [57], and Statgraphics [58], which design and analyze response surface methodology (RSM) as an efficient way to deal with the limitations of the classical method [55]. RSM, a multivariable system, [59], is a useful technique for the optimization and modeling of the effects of multiple variables and their responses, in which all factors are varied simultaneously [55,60]. These software applications have some disadvantages: the functionality of RSM's ccd.pick function is not provided by them and they lack RSM's capabilities in the generality of central-composite designs (CCD) that RSM can create. The R software removes these limitations [61,62]. In R software, RSM covers the most standard first and second order designs and methods for one response variable; but it covers those reasonably well, and it could be expanded in the future. In this software, RSM has the dual aim of finding the optimum settings for the variables and seeing how the variables perform over the whole experimental domain, including any interactions [62,63]. On the other hand, the R software has the following features: (i) it provides estimates of all the coefficients in the model (ii) it requires as few experiments as possible (iii) it provides a test for lack of fit (i.e. how well the model fits the data) (iv) it allows blocking of experiments (v) it allows specified variance criteria for estimated coefficients and estimated responses to be met [61]. Therefore, in the present work, the modification of GO with 8-HQ (that has not yet been reported in detail) was done based on the idea that this chemical will improve the GO adsorption capacity for Cr (VI). Thus, the optimization and modeling (by R software) of the removal study of Cr (VI) in water solutions was investigated using 8-HQ/GO. Based on the above-mentioned facts, the present study was undertaken: (i) to optimize and find an appropriate functional relationship between the response (Cr (IV) removal efficiency) and related input variables (solution pH, time, adsorbent dose, Cr (IV) concentration) by RSM using central composite design (CCD) (ii) to obtain optimum conditions of the model equation predicted by RSM using the Solver "Add-ins" (iii) to study various isotherm models and kinetic equations to identify the possible adsorption mechanism, and (iv) to determine adsorption thermodynamics of Cr (VI) on the studied adsorbent.

2. Materials and methods

2.1. Chemicals

All chemicals were of reagent grade and doubly distilled water (DDW) was used throughout this work. Natural graphite powder, 8-HQ, potassium permanganate ($KMnO_4$), H_2SO_4, H_2O_2, $FeCl_3.6H_2O$,

$FeSO_4.7H_2O$, NH_4OH, potassium dichromate ($K_2Cr_2O_7$) and sodium nitrate ($NaNO_3$) were provided by Merck Co. (Germany). The pH of the Cr (VI) solution was adjusted to the desired values by adding 0.1 M NaOH (BDH chemicals Co, UK) and/or HCl (37%, Merck Co) through a manual syringe injection. The working solutions of the Cr (VI) were obtained by appropriate dilution of the stock solution.

2.2. Synthesis of GO, magnetic GO-Fe_3O_4 nanocomposite and 8-HQ - functionalized GO-Fe_3O_4 nanocomposite

GO sheets and magnetic GO -Fe_3O_4 nanocomposite were prepared by a modified Hummers method [63]. Firstly, natural graphite powder (5 g) was added into a 500.0 mL flask containing 115 mL H_2SO_4 (98%,) and stirred for 30 min. Next, 2.5 g $NaNO_3$ was added into the mixture and stirred vigorously to avoid agglomeration. After that, 15 g $KMnO_4$ and 50 mL H_2O_2 solution (30%) was gradually added into the flask and then cooled by immersion in an ice bath. The mixture was stirred for 45 min, then HCl (1 mol L^{-1}) was applied to wash the resultant suspension and it was collected by centrifugation. To prepare the GO-Fe_3O_4 nanocomposite [64,65], ultrasonic irradiation was used for 5 min in order to disperse 0.1 g of GO in 25 mL of deionized water. Then 256.5 mg of $FeCl_3.6H_2O$ and 132 mg of $FeSO_4 \cdot 7H_2O$ were added in 25 mL of deionized water. The obtained solution was added to the GO solution and stirred for 30 min. After adding the 2 mL NH_4OH aqueous solution (25%) into the mixture (drop by drop), the mix was kept under constant stirring at 90 °C for 4 h. Finally, the obtained product was washed with acetone and separated by a magnet. It was vacuum-dried at 40 °C for 4 h. IR spectroscopy and thermogravimetric analysis were applied to confirm the formation of GO-Fe_3O_4 nanoparticles (GO-Fe_3O_4 NPs). The whole process was performed under atmospheric nitrogen. To synthesis the 8-HQ - functionalized GO-Fe_3O_4 nanocomposite (8-HQ-GO-Fe_3O_4), a saturated solution of 8-HQ was prepared and sonicated for 2 h [48,64]. To remove the undissolved 8-HQ, it was filtrated through a 0.45-μm filter membrane. After that, 1.0 g of GO-Fe_3O_4-NPs was added into the solution and the mixture was stirred for 2 days. To remove excess 8-HQ (until becoming colorless), the mixture was washed with deionized water. The solid GO-Fe_3O_4-NPs were collected using an external magnetic field. Finally, the prepared product was washed and then dried in an oven at 60 °C overnight. IR spectroscopy, scanning electron microscopy, and thermal analysis were applied to confirm the formation of 8-HQ-GO-Fe_3O_4. The schematic of the 8-hydroxyquinoline modified with graphene oxide is shown in Fig. 1.

2.3. Sorbent characterization and analytical methods

The surface structure of 8-HQ- GO-Fe_3O_4 was analyzed by scanning electron microscopy (SEM) coupled with energy dispersive X-ray analysis (EDAX) using the Cambridge-Leo system at 15 kV with background subtraction with a summation of 240 scans. In addition, FT-IR analysis was performed on the samples that were encapsulated with KBr to prepare translucent sample disks using a Fourier Transform Infrared spectrophotometer (Bruke EQUINOX 55 Germany). The infrared spectra were measured within a range of 40–4000 cm^{-1}.Thermo gravimetric analysis on the GO-Fe_3O_4 and 8-HQ-GO-Fe_3O_4 nanocomposite in the temperature range of 30 to 800 °C is shown in Fig. 6(a,b). According to the TGA analysis, these nanocomposites are stable up to 800 °C. The weight losses occurred at 250 °C, is due to the loss of residual water and pyrolysis of oxygen-containing groups in the surface of nanosorbents. Also, GO-Fe_3O_4 and 8-HQ-GO-Fe_3O_4 nanocomposite have lost 1.06 mg and 2.75 mg of their weights at about 800 °C (The initial weight is the same). These observations indicated that the magnetic graphene oxide nanocomposite (GO-Fe_3O_4) was successfully modified by 8-hydroxyquinoline [66,67]. All samples were analyzed for residual Cr (VI) concentration using graphite furnace atomic absorption spectrometer (GFAAS, Buck Scientific, Inc. 210VGP model, USA). All experiments were performed at least twice and the averages were reported.

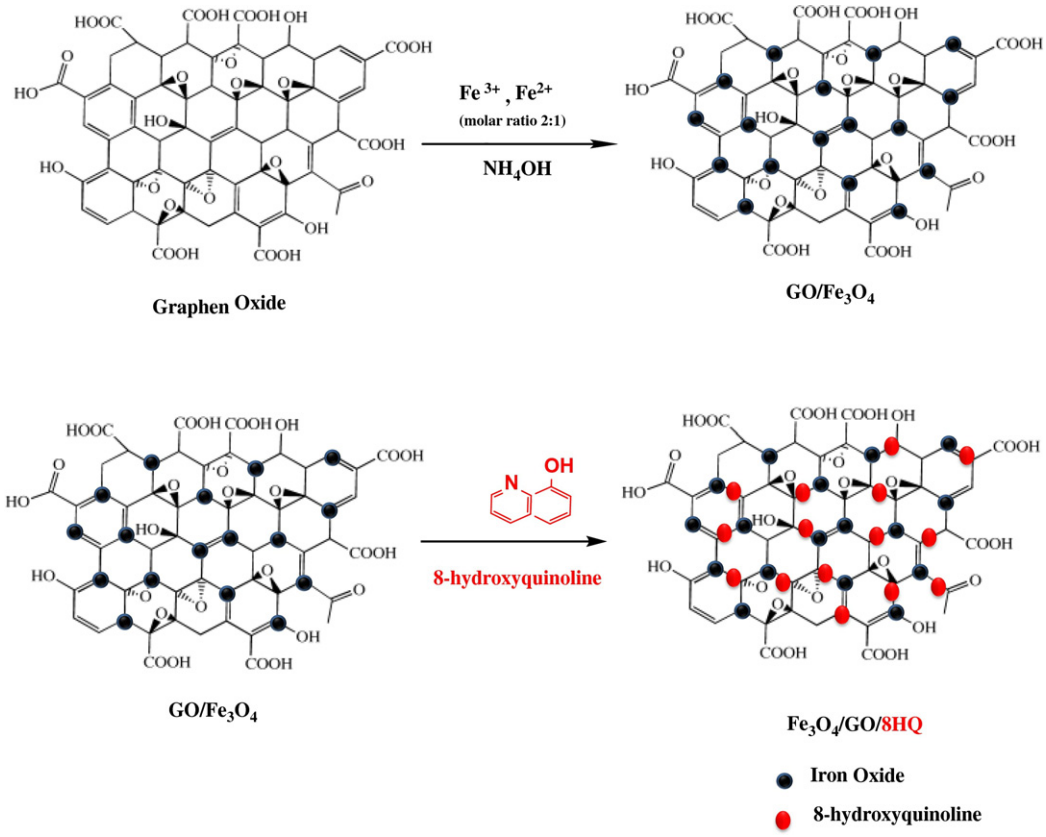

Fig. 1. Schematic representation of Synthesis of GO, magnetic GO-Fe_3O_4 nanocomposite and 8-HQ - functionalized GO-Fe_3O_4 nanocomposite.

Table 1
Actual and coded values of independent variables used for experimental design.

Variable	Symbol	Coded level		
		−1	0	1
			Real values	
pH	X_1	2	5	8
8-HQ/GO dose (g L^{-1})	X_2	10	55	100
Time (min)	X_3	2	91	180
Cr (VI) concentration (mg L^{-1})	X_4	1	5.5	10

The analysis was carried out using calibration curves with correlation coefficients (R^2) of 0.999. Standards were re-measured during each set of experiments to assess accuracy and stability in the measurements and to make sure of adequate instrument performance [68].

2.4. Adsorption studies

Adsorption behavior of Cr (VI) by 8-HQ- GO-Fe_3O_4 was investigated using batch study. All the experiments were carried out using glass Erlenmeyer 250 mL flasks containing 200 mL Cr (VI) solution at room temperature (25 ± 1 °C). The Cr (VI) solutions with the desired concentrations were prepared by dilution of the stock solution immediately before use. The effect of various parameters such as pH, 8-HQ-GO-Fe_3O_4 dose, time and initial Cr (VI) concentration was evaluated according to the design developed by RSM. The initial pH of the solution was adjusted in the desired amount and the required dosage of the adsorbent was added inside the Erlenmeyer flasks with a certain concentration of Cr (VI). The flasks were shaken with an orbit incubator shaker (Melrose park, ILL, No3595, USA) operated at 180 rpm. At specified time intervals, samples were withdrawn from the solution, centrifuged (at 3000 rpm

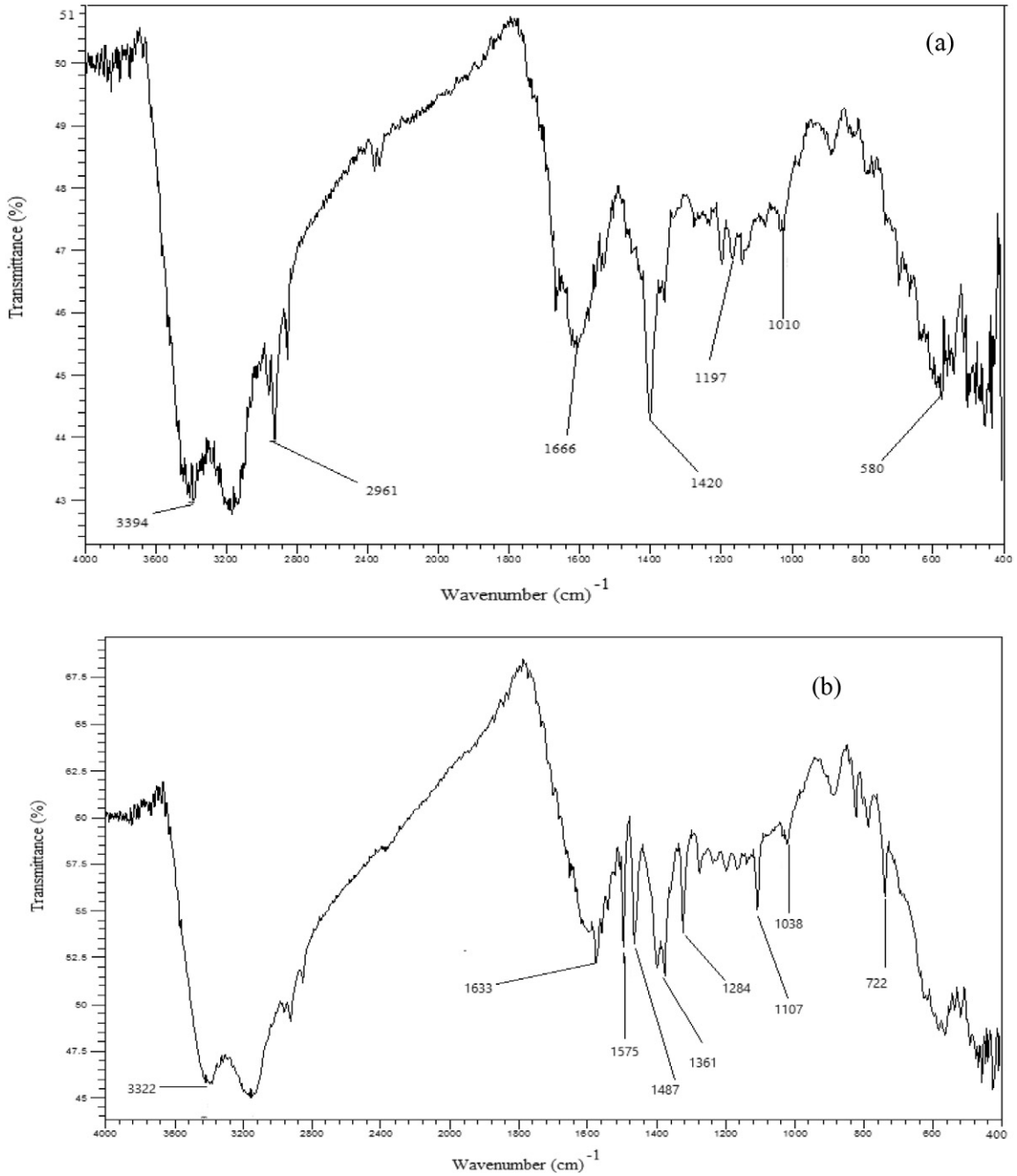

Fig. 2. The FTIR spectra for GO-Fe_3O_4 nanocomposite (a) 8-HQ - functionalized GO-Fe_3O_4 nanocomposite (b).

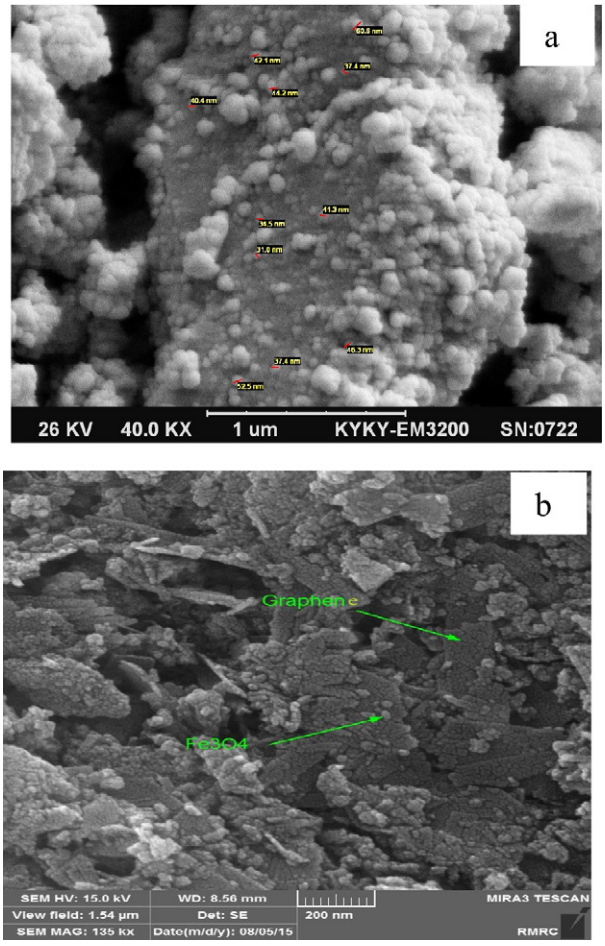

Fig. 3. SEM images of GO (a) and 8-HQ - functionalized GO-Fe_3O_4 nanocomposite (b).

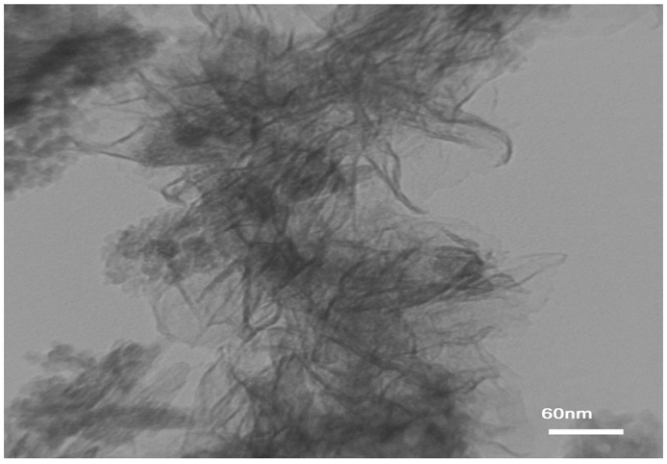

Fig. 4. TEM image of 8-HQ - functionalized GO-Fe_3O_4 nanocomposite.

for 5 min), filtered through 0.22 μm syringe filters, and then analyzed for residual Cr (VI) concentrations using a graphite furnace atomic absorption spectrometer (GFAAS, Buck Scientific, Inc. 210VGP model, USA).

2.5. Factorial experimental design and the optimization of parameters

The response surface methodology using CCD (Box-Wilson model) as a useful statistical tool was chosen to consider the composition effect of input-independent factors (pH (x_1), 8-HQ/GO dose (x_2), time (x_3) and Cr (VI) concentration (x_4),) and an output-dependent response variable (removal efficiency (Υ)) [69]. The R software for windows (version 3.0.3:6 March 2014) was used for this purpose [61,69]. The CCD in the R software is an orthogonal design consisting of a factorial 2-level design (with 2^k points that form the base design) to which is added a 'star' design (axial points) with 2k points plus centre points, where k is the number of variables [70]. The design for 4 variables is given in Table 1. The levels for each variable are shown in coded and uncoded form. 28 runs per experimental design were obtained from the R software using 16 factorial points and 12 center points. A response surface was fitted using the special functions including the first-order response-surface (including FO (first-order) term), two-way interactions (including FO and TWI (two-way interaction) terms) and full second-order models (by adding PQ (the pure quadratic) term) to the above model with interaction. Although SO (second-order) model is shorthand for a model with FO, TWI, and PQ terms, these functions are significant in the specification of the response-surface portion of the model [61]. These functions were fitted to the data in order to obtain a suitable response-surface model. To achieve more fitting, some terms were removed from the model and the quadratic model was reduced [69]. The accuracy of model fitting was evaluated by ANOVA analysis [70]. In general, the model with the greater F-value, the smaller *p*-value and insignificant lack of fit (or more lack of fit) was selected as the appropriate model [70,71]. Eq. (1) was used to describe the effect of variables in terms of linear, quadratic, and interaction models:

$$\Upsilon = b_0 + \sum_{i=1}^{k} b_i X_i + \sum_{i=1}^{k} b_{ii} X_i^2 + \sum_{i=1}^{k-1} \sum_{j=1}^{k} b_{ij} X_i X_j + C \quad (1)$$

where b_0 is intercept value, b_i, b_{ii}, and b_{ij} refer to the regression coefficient for linear, second order, and interactive effects, respectively, X_i and X_j are the independent variables, and C denotes the error of prediction [56,59]. Finally, to obtain the optimum conditions, the Solver "Add-ins" were applied using effective parameters to write the model equation as predicted by RSM [61,69].

2.6. Kinetic, thermodynamic, and isotherm studies

Equilibrium experiments were conducted under the optimum conditions obtained from the model (pH 6.5, 8-HQ-GO-Fe_3O_4 dose, 98.4 g L^{-1}), an initial Cr concentration of 1 to 10 mg L^{-1} at a temperature of 15–35 °C with the total volume of 200 mL in a 250 mL Erlenmeyer flask. The mixture was shaken for 3 h at 200 rpm and environmental temperature. To determine the relationship between equilibrium capacity and equilibrium concentration, adsorption results were then analyzed and fitted by the Langmuir, Freundlich and Temkin isotherm models. Linear formulas used for isotherm models are shown below:

$$\frac{c_e}{q_e} = \frac{1}{q_m b} + \frac{1}{q_m} c_e \quad (2)$$

$$R_L = \frac{1}{[1 + bc_0]} \quad (3)$$

$$\log q_e = \log k_f = \frac{1}{n} \log c_e \quad (4)$$

$$q_e = B_1 \ln(k_t) + B_1 \ln(C_e) \quad (5)$$

Where q_e is the equilibrium amount of the adsorbate (mg g^{-1}), C_e is the equilibrium concentration of the adsorbate (mg L^{-1}), q_m is the amount of Cr (VI) adsorbed at complete monolayer (mg g^{-1}) and b is the Langmuir constant related to the binding site (L/mg). The important feature of the Langmuir model can be described based on the R_L parameter expressed in Eq. (3). The value of R_L indicates that the adsorption is

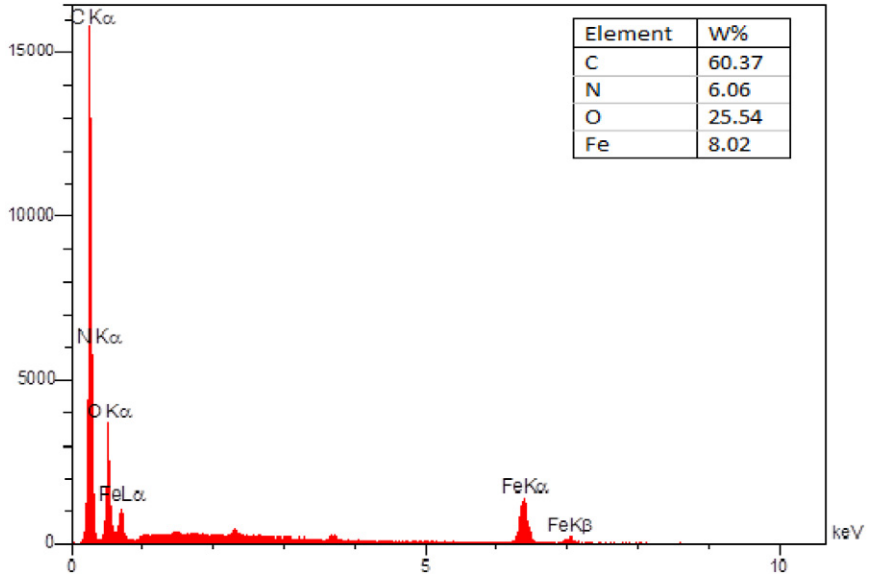

Fig. 5. Energy dispersive x-ray spectroscopy (EDAX) of 8-HQ - functionalized GO-Fe_3O_4 nanocomposite.

either unfavorable ($R_L > 1$), linear ($R_L = 1$), favorable ($0 < R_L < 1$) or irreversible ($R_L = 0$). C_0 is the highest initial concentration of Cr (VI) ions (mg L^{-1}). K_f ($mg^{1-1/n}/L^{1/n}/g$) and 1/n are the Freundlich constants that are related to the adsorption capacity and intensity, respectively. For a favorable adsorption, the value of the Freundlich constant (n) should be in the range of 1–10. The linear form of the Temkin model is given by Eq. (5), where $B_1 = RT/b_1$ (R is the universal gas constant [8.314 kJ/-kmol K] and T[K] is the absolute temperature), b_1 is the adsorption heat (kJ mol^{-1}) and k_t is the equilibrium binding constant (L/g) corresponding to the maximum binding energy. A high value for b_1 shows a fast sorption of the adsorbate at the initial stage. Similarly, a low k_t value is related to the weak bonding of the adsorbate onto the medium. By plotting q_e versus ln (C_e), b_1 and k_t can be deduced from the slope and the intercept of this curve, respectively. The optimum conditions obtained from the model were used to investigate the kinetic model. For this purpose, the adsorbent was added onto 200 mL Cr solution containing 2–10 mg L^{-1} solute for 360 min. In this study, four types of kinetic models, including pseudo-first order, pseudo-second order, Elovich and intra-particle diffusion models, were considered. The liner formulas of the mentioned kinetic models are presented below:

$$\log q_e - q_t = \log q_e - \frac{k_1}{2.303} t \tag{6}$$

$$\frac{t}{q_t} = \frac{1}{k_2 q_e^2} + \frac{1}{q_e} t \tag{7}$$

$$q_t = \left(\frac{1}{\beta}\right) \ln(\alpha\beta) = \left(\frac{1}{\beta}\right) \ln t \tag{8}$$

$$q_t = k_d t^{1/2} + I \tag{9}$$

where q_e (mg g^{-1}) and q_t are the amounts of Cr (VI) adsorbed at equilibrium and time t(min), respectively and k_1(min^{-1}) is the rate constant in the pseudo-first order adsorption model. k_2 (g mg^{-1} min^{-1}) is the rate constant in the pseudo-second order adsorption model. The parameters of α (mg g min^{-1}) and β (g mg^{-1}) are the rate of chemisorption at zero coverages and the surface coverage and activation energy of chemisorption, respectively. The parameter of q_t (mg g^{-1}) is the amount of Cr (VI) adsorbed at time t, k_d is the intra-particle diffusion rate constant (mg g^{-1} $min^{-1/2}$) and I is a constant that gives an idea about the thickness of the boundary layer. The initial adsorption rate, h_0, is determined as follows (mg g^{-1} min^{-1}):

$$h_0 = k_2 q_e^2 \tag{10}$$

The temperature influence on Cr (VI) adsorption onto HQ- GO-Fe_3O_4 was investigated in the range of 15–35 °C. The Arrhenius equation was applied to study the nature of the adsorption as follows:

$$\ln k_d = \ln A_0 - \frac{E_a}{RT} \tag{11}$$

where A_0 is the frequency factor or the independent temperature factor (g mol^{-1} min^{-1}), E_a is the activation energy of adsorption (kJ mol^{-1}), R is the gas law constant (8.314 J mol^{-1} K^{-1}), and T is the solution absolute temperature (K). For physical adsorption, E_a is lower than 40 kJ mol^{-1} while for chemisorption it is higher than 40 kJ mol^{-1}. E_a and A_0 can be calculated from the slope and the intercept of the linear plot of ln k versus 1/T, respectively. Thermodynamic parameters were determined using the equilibrium constant k_d (q_e/C_e) for temperatures ranging from 15 to 35 °C. The Gibbs free energy (ΔG° (kJ mol^{-1})) is the fundamental criterion of spontaneity which is calculated from the following equation.

$$\Delta G^0 = -RT \ln K_d \tag{12}$$

The parameters of enthalpy (ΔH⁰ (kJ mol^{-1})) and entropy (ΔS⁰ (kJ mol^{-1} K^{-1})) were determined from the following equation. The slope and the intercept of the linear plot of ln k versus 1/T was used for the calculation of ΔH⁰ and ΔS⁰ parameters, respectively.

$$\ln k_d = \frac{\Delta S^0}{R} - \frac{\Delta H^0}{RT} \tag{13}$$

3. Results and discussion

3.1. Characterization results

Detailed information about the formation of 8-HQ-GO-Fe_3O_4 was obtained by FT-IR spectroscopy, SEM, EDS, TEM and TGA methods. IR spectrum of GO-Fe_3O_4 was characterized as follows (cm^{-1}): 580 (Fe—O), 1666 (C═O), 1197 (C—O—C) and 3394 (COOH). The

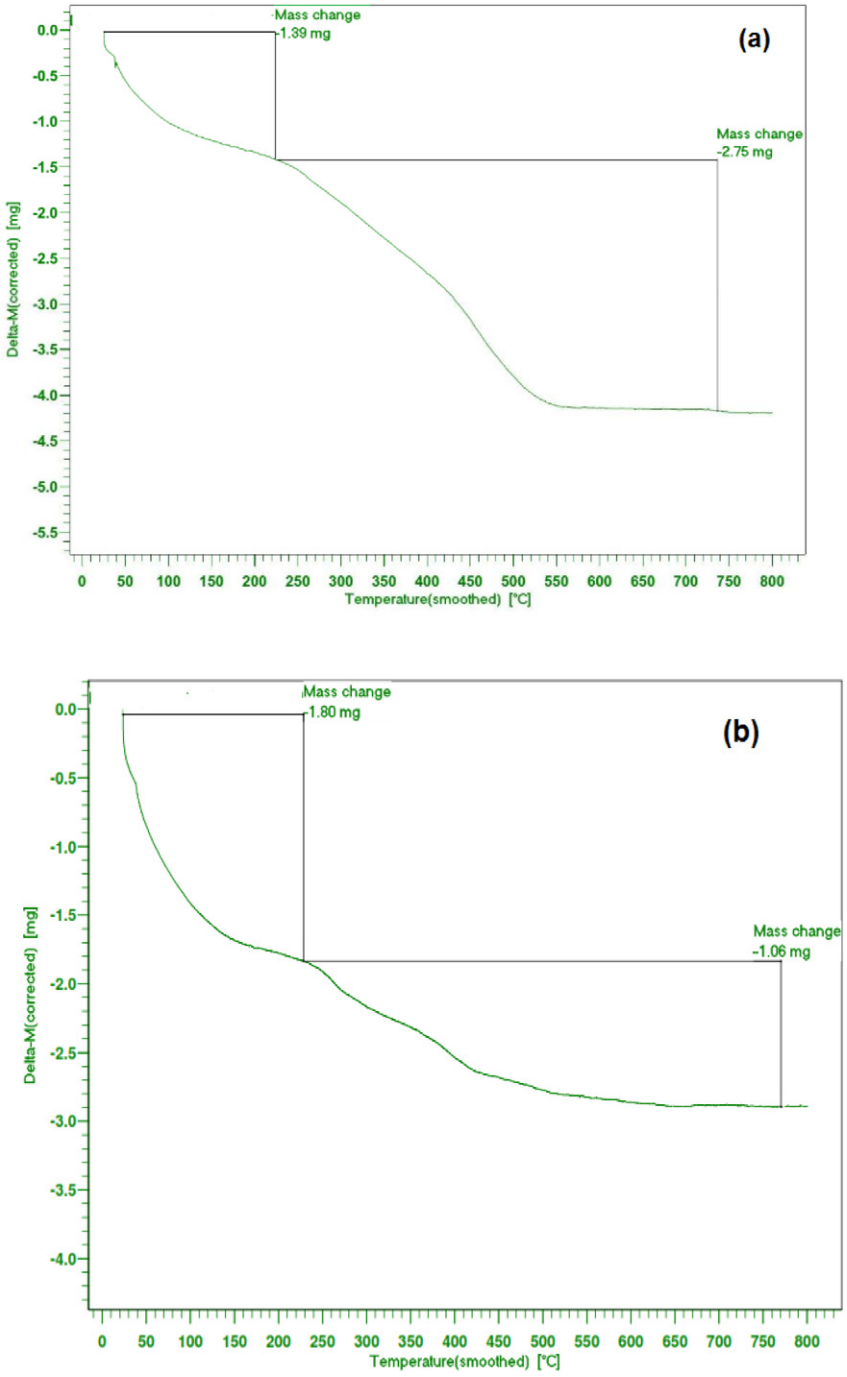

Fig. 6. The TGA plots of (a) GO-Fe_3O_4 and (b) magnetic GO-8HQ nanocomposite.

modification of GO-Fe_3O_4 with 8-HQ signals at 1575 cm^{-1} (C = N) and 1107 cm^{-1} (C—N) showed GO-Fe_3O_4 was successfully modified by 8-HQ (Fig. 2). In order to show the structure of the synthesized sorbent, the morphology of GO and 8-HQ-GO-Fe_3O_4 was investigated by SEM. The SEM pattern in Fig. 3 showed that iron oxide nanoparticles were successfully coated on the surface of graphene oxide. A closer observation of TEM images with higher magnifications in Fig. 4 made it clear to observe the ordered mesostructures. Morphological of 8-HQ-GO-Fe_3O_4 reveals a homogeneous structure. EDAX spectrum taken from the 8-HQ-GO-Fe_3O_4 is presented in Fig. 5. The quantitative analysis gives weight ratios of Fe (8.02%), C (60.37%), O (25.54%) and N (6.06%). The results showed the presence of 8-HQ on the surface of the GO-Fe_3O_4. Thermo gravimetric analysis on the GO-Fe_3O_4 and 8-HQ-GO-Fe_3O_4 nanocomposite in the temperature range of 30 to 800 °C is shown in Fig. 6(a,b). According to the TGA analysis, these nanocomposites are stable up to 800 °C. The weight losses occurred at 250 °C, is due to the loss of residual water and pyrolysis of oxygen-containing groups in the surface of nanosorbents. Also, GO-Fe_3O_4 and 8-HQ-GO-Fe_3O_4 nanocomposite have lost 1.06 mg and 2.75 mg of their weights at about 800 °C (The initial weight is the same). These observations indicated that the magnetic graphene oxide nanocomposite (GO-Fe_3O_4) was successfully modified by 8-hydroxyquinoline.

3.2. Generating a CCD design and fitting a response-surface model

Based on the Box and Wilson design, the 28 runs, obtained from the R software, showing the independent variable (coded and uncoded) and dependent response (experimental and predicted) levels are

Table 2
Central composite design matrix with coded and uncoded values of the independent variables and experimental and predicted values of the response.

Sl.no.	Coded values				Un coded values				% Removal	
	X_1	X_2	X_3	X_4	X_1	X_2	X_3	X_4	Expt. (ϒ)	Pred. (ϒ)
1	1	1	1	−1	8	100	180	1	97.10	91.22
2	1	−1	1	−1	8	10	180	1	79.70	80.87
3	0	0	0	0	5	55	91	5.5	73.30	71.46
4	−1	−1	−1	−1	2	10	2	1	28.99	28.69
5	0	0	0	0	5	55	91	5.5	77.25	71.46
6	0	0	0	0	5	55	91	5.5	72.11	71.46
7	0	0	0	0	5	55	91	5.5	76.29	71.46
8	−1	−1	−1	1	2	10	2	10	17.54	16.27
9	−1	1	−1	1	2	100	2	10	24.54	22.57
10	0	0	0	0	5	55	91	5.5	71.22	71.46
11	0	0	0	0	5	55	91	5.5	74.89	71.46
12	−1	1	1	1	2	100	180	10	37.60	33.50
13	0	0	0	0	5	55	91	5.5	72.17	71.46
14	1	−1	−1	1	8	10	2	10	52.50	51.44
15	0	0	0	0	5	55	91	5.5	74.28	71.46
16	0	0	0	0	5	55	91	5.5	71.98	71.46
17	−1	1	1	−1	2	100	180	1	54.80	49.97
18	0	0	0	0	5	55	91	5.5	72.18	71.46
19	0	0	0	0	5	55	91	5.5	76.30	71.46
20	0	0	0	0	5	55	91	5.5	73.31	71.46
21	−1	−1	1	1	2	10	180	10	26.74	27.20
22	1	1	−1	−1	8	100	2	1	74.55	74.21
23	1	1	−1	1	8	100	2	10	63.55	57.74
24	−1	1	−1	−1	2	100	2	1	39.50	39.04
25	1	1	1	1	8	100	180	10	79.54	74.75
26	−1	−1	1	−1	2	10	180	1	40.30	39.62
27	1	−1	−1	−1	8	10	2	1	65.45	63.86
28	1	−1	1	1	8	10	180	10	73.14	68.45

presented in Table 2. Three special models (first-order, two-way interactions and full second-order models) of RSM were applied and tested to fit the data. Each model is presented with the usual summary for an lm object that is followed by some particular additional information. The summery of each model introduces information about lack of fit, multiple R-squared, adjusted R-squared, F-statistic, *p*-value and AIC. The results are presented in Table 3. These terms were applied in order to specify the response-surface portion of the model. Also, the summery of the model presents information about the direction of the steepest ascent (data not shown), since the dataset is coded. The data object, the steepest-ascent information, is also presented as a stationary point in the original (data not shown) [66,68,69]. The stationary point in the original is response-surface experimentation, clear evidence of a nearby set of optimal conditions. The lack of fit value of the model determines data variation around the fitted model and must be insignificant in a well-fitted model. The comparison of the three mentioned models showed a breakdown of lack of fit (significant) and small *p* value for lack-of-fit for all models (Table 3), although the full second-order model showed a higher lack-of-fit than the two previous models. Therefore, the stationary point in the original unit information for these models is of little use. In paying attention to the obtained results from the three previous models, we tried to apply a reduced model, in order to achieve a model with higher lack-of-fit (insignificant). Thus, the reduced full second-order model was obtained with the removal

Table 4
Analysis of variance (ANOVA) for the reduced quadratic model.

Model formula in RSM	DF	Sum of squares	Mean square	F-value	Probability (P)
First-order response (x_1, x_2, x_3, x_4)	4	8320.2	2080.05	491.2739	<2.2e-16
Two-way interaction response (x_1, x_2, x_3, x_4)	6	68.9	11.48	2.7119	0.05179
Pure quadratic response (x_1)	1	2826.3	2826.34	667.5348	1.789e-14
Residuals	16	67.7	4.23	–	–
Lack of fit	5	23.4	4.68	1.1598	0.38722
Pure error	11	44.4	4.03	–	–

Multiple R-squared: 0.99, adjusted R-squared: 0.98, predicted $R^2 = 0.989$, F-statistic: 240.8 on 11 and 16 DF, *p*-value: 1.336e-15, AIC = 48.74.

of (x_2, x_3, x_4) from the PQ term. The lack of fit value of the reduced model was non-significant ($p \approx 0.38$) that indicated a well-fitted model. The summary of the reduced model indicated the eigenvalues are of mixed sign, indicating that it is a saddle point (data are not shown) [61].

3.3. The development of regression model equation and analysis of variance

Analysis of variance (ANOVA) is a statistical technique that can be used to check model adequacy [58–61]. We present the ANOVA results for central composite design in Table 4. Five parameters of the *P*-value, F-value, R^2, lack of fit and AIC were applied to appraise model adequacy. *P*-value and F-value are related to the significance of the model terms and more significant effects of the model terms (P valve parameter is contrary to F valve parameter). Lower *P*-value (1.33×10^{-15}), higher F-value (240.4), higher R^2 (multiple R-squared: 0.994, adjusted R-squared: 0.989), insignificant lack of fit (0.38) and lower AIC (48.74) indicate that the reduced full second-order model was highly significant for Cr (VI) removal by 8-HQ-GO-Fe_3O_4 and it also represents the satisfactory agreement between the model and experimental data [64,65]. The results indicate the R-squared value of the model is very close to the adjusted R-squared value that expresses a good chance for significant terms to be included in the model [60,61]. Also, the presence of significant terms in the model was proved with good agreement between R^2_{adj} (0.98) with R^2_{pred} (0.98) that is shown in Fig. 7 [69]. Therefore, the model can be used for prediction and optimization. The results of regression analysis of the reduced quadratic model with coded and uncoded values of the independent variables are given in Table 5. As Table 5 shows, it was found that independent variables x_1, x_2, x_3 x_4, the interaction (x_1: x_3 and x_2: x_4) and also pure quadratic response for x_1 (x_1^2) have significant effects (*p*-values < 0.05) on Cr (VI) removal; therefore, these terms could be entered into the model formulation. The terms of x_4, x_2: x_4, x_1^2 showed an antagonistic effect on the model, while other terms had a synergistic effect on the response prediction by the model. The obtained equations from the quadratic model, for both coded and actual factors of parameters are presented below:

The final equation in terms of coded factors:

$$\Upsilon = 73.77 + 19.72\,X_1 + 5.42\,X_2 + 7.64\,X_3 - 6.57\,X_4 - 20.3\,X_1^2 + 1.53\,X_1X_3 - 1.01\,X_2X_4 \quad (14)$$

Table 3
The comparison of different moles of RSM for fitting a response-surface model.

	Multiple R-squared	Adjusted R-squared	F-statistic	*p*-Value	AIC	Lack of fit
First-order response-surface model	0.73	0.69	16.15 on 4 and 23 DF	1.989e-06	140.57	2.974e-08
Two-way interactions model	0.74	0.59	4.928 on 10 and 17 DF	0.00201	151.87	2.487e-09
Second-order model	0.84	0.72	140.5 on 9 and 15 DF	1.2×10^{-9}	38.74	0.1
Reduced full second-order model	0.99	0.98	240.8 on 11 and 16 DF	1.2×10^{-9}	48.74	0.38

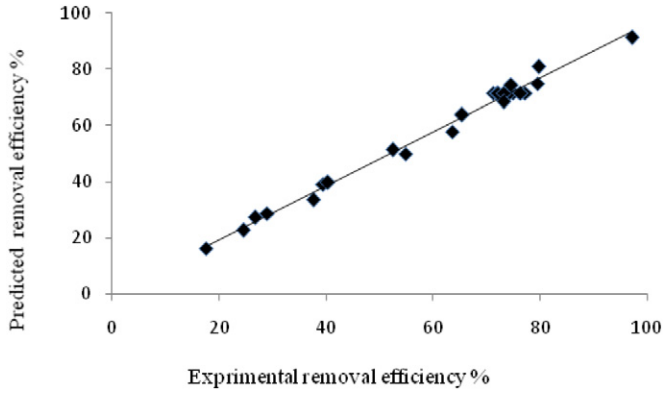

Fig. 7. Experimental arsenite removal vs. predicted removal efficiency.

The final equation in terms of actual factors:

$$\Upsilon = -18.95 + 28.35\,X_1 + 0.12\,X_2 + 0.05\,X_3 - 1.33\,X_4 - 2.25\,X_1^2 + 0.0057\,X_1X_3 - 0.005\,X_2X_4 \quad (15)$$

3.4. Process optimization and confirmation

As results mentioned in previous sections indicate, the reduced full second-order model was selected as a well-fitted model. Therefore, the optimization process was conducted using the reduced model. The mixed signs of the eigenvalue (negative and positive) revealed that it is neither a maximum nor a minimum amount. The stationary point in the original units for pH, adsorbent dose, time and initial Cr (VI) concentration were 5.9, 97.2 g L^{-1}, 176.4 min and 1 mg L^{-1} respectively, that can be clear experimental evidence of a nearby set of optimal conditions and we should probably collect some confirmatory data near this estimated optimum to make sure. To confirm this issue and obtain optimum conditions, the model predicted by RSM, the Solver "Add-ins", was applied using the effective parameters [61,69]. This method uses iterative numerical methods to approximate an optimal solution, starting from initial guesses and making 'improved' guesses till an optimal solution fitting the constraints is found. The 'Solver' utility in Excel is a convenient way to do this. To set it up, we need to enter the coefficients for the uncoded model. We also need initial guesses (values estimated from the response surfaces are good starting points). A value of the yield is then calculated, using the regression equation. We then set up the solver to maximize this value of the yield by varying the three variables subject to the constraints [69]. The Solver method is designated by parameters of pH (2–8), adsorbent dose (10–100 g L^{-1}), time (2–180 min) and initial Cr (VI) concentration (1–10 mg L^{-1}). The maximum removal efficiency was estimated as 95.77% to involve all parameters simultaneously. The predicted optimal conditions by the Solver method in the maximum removal efficiency were achieved at the initial Cr (VI) concentration of 1 mg L^{-1}, an adsorbent dose of 98.4 (g L^{-1}), time of 178.4 (min) and a pH of 6.55 that was very close to the stationary point in the original units. An additional experiment was carried out (at recommended conditions by RSM), to confirm the validity of the predicted optimum conditions. As Table 6 shows, it is found that the experimental findings for the response is in good agreement with model predictions [70,71], with a low error of 1.92%, and a low standard deviation of ± 1.66%.

3.5. Response surface methodology and contour plotting

Contour plotting was applied to express the interactive effect of the dependent variables on the removal efficiency. The effects of pH (2–8) and time (2–180 min) on the adsorption of Cr (VI) ions over 8-HQ-GO-Fe_3O_4 were simultaneously monitored at constant Cr (VI) ions concentration and presented in Fig. 8a. The pH has an important role during the adsorption process, because it can affect the solubility of the metal ions, the degree of ionization of the sorbate and the functional groups of the sorbent controlling the metal ion sorption process. As can be seen from the Fig. 8a, an increase of pH from 2 to 6.5 promoted removal efficiency, while an increase of pH above 6.5 caused a decrease in the adsorption of Cr on 8-HQ-GO-Fe_3O_4. Wang et al. reported the pH_{pzc} (point of zero charge) of GO to be 3.8; therefore, the surface charge of GO is negative at pH > 3.8 that the positive Cr (VI) ions are easily adsorbed on the negatively charged GO surfaces through electrostatic attraction. This can be reasonable for the high sorption of Cr.

(VI) on GO at pH > 3.8. Given that adsorption of Cr (VI) on 8-HQ-GO-Fe_3O_4 is independent of ionic strength and dependent on pH values, the sorption is mainly dominated by inner-sphere surface complexation [72,73]. The maximum Cr sorption occurred for a pH in the range of 5–6.5 with increasing time, at fixed adsorbent dose and initial Cr concentration of 55 g L^{-1} and 5.5 mg L^{-1}, respectively. In general and surprisingly, the 8-HQ-GO-Fe_3O_4 adsorbent exhibited relatively low sorption capacities for Cr ions at the values of pH ˃ 6.5, which suggests that a weak attraction took place between the adsorbent surface and the negative ions. The different pH conditions enhance the reduction of Cr (VI) to Cr (III) that can be proved by the diphenylcarbazide method [74]. Cr (III) can be in the different forms of Cr $(H_2O)_3^{3+}$, Cr $(H_2O)_2(OH)^{2+}$, or Cr $(H_2O)(OH)^{2+}$ and so on. These Cr forms can create a Cr-HQ-GO-Fe_3O_4 complex compound that can be affected by the pH conditions. Under natural conditions, the reaction activity between the analytes and the chelating agent is enhanced, and the formation of a Cr-8-HQ complex compound is promoted. In basic conditions (pH > 6.5), the Cr-8-HQ chelate will decompose. In addition, in the basic region, deposition plays a predominant role in the removal of Cr ions from solutions. It can be explained by the fact that the Cr species start to hydrolyze and precipitate into chromium hydroxide at pH > 6.5 [25]. Moreover, the interaction effect of time as one of the significant parameters for the successful use of the adsorbent for practical applications was investigated. As can be seen from Fig. 8a, at a fixed pH, an increase of time from 2 to 150 promoted Cr adsorption, as with increasing time from 2 to 150, removal efficiency increased from 70 to 85% for a pH of 6.5 and at a fixed adsorbent dose and an initial Cr concentration of 55 g L^{-1} and 5.5 mg L^{-1}, respectively. In research conducted by Wang et al. graphene oxides and graphene oxide-based

Table 5
Regression analysis of the reduced quadratic model with coded and uncoded values of the independent variables.

Model term	Coded values				Un coded values			
	Coefficient estimate	Std. error	t-Value	*p*-Value	Coefficient estimate	Std. error	t-Value	*p*-Value
(Intercept)	73.77333	0.59400	124.1981	<2.2e-16	−1.895e + 01	3.056e + 00	−6.201	1.27e-05
X_1	19.72000	0.51442	38.3347	<2.2e-16	2.835e + 01	9.541e-01	29.713	2.00e-15
X_2	5.42625	0.51442	10.5484	1.300e-08	1.293e-01	2.873e-02	4.499	0.000365
X_3	7.64375	0.51442	14.8591	8.802e-11	5.115e-02	1.503e-02	3.402	0.003643
X_4	−6.57750	0.51442	−12.7863	8.160e-10	−1.333e + 00	2.873e-01	−4.640	0.000272
X_1: X_3	1.53500	0.51442	2.9840	0.008768	5.749e-03	1.927e-03	2.984	0.008768
X_2: X_4	−1.01250	0.51442	−1.9682	0.066617	−5.000e-03	2.540e-03	−1.968	0.066617
X_1^2	−20.30208	0.78578	−25.8367	1.789e-14	−2.256e + 00	8.731e-02	−25.837	1.79e-14

Table 6
Experimental and predicted values of the responses at the optimal levels predicted by RSM.

pH	8-HQ/GO dose (g L^{-1})	Time (min)	Cr (VI) concentration (mg L^{-1})	Cr (VI) removal (%)		Error (%)	STDEV (±%)
				Predicted (%)	Experimental (%)		
6.55	98.4	178.4	1	95.77	93.25	−1.92	1.66

nanomaterials applied in radionuclide removal from aqueous solutions. They revealed that the extent of U(VI) reduction to U(IV) was significantly increased with increasing reaction time, suggesting that part of surface adsorbed U(VI) was reduced to U(IV) on nZVI/rGO composites, and the reduction of U(VI) was increased with increasing aging time. They proved the presence of multimeric surface complexes, and $U_{IV}O_2$ precipitates were formed on the surface of the composites, which was important for the application of nZVI/rGO composites in the elimination, immobilization and reduction of U(VI) to U(IV) in environmental pollution management. After the reduction of U(VI) to U(IV), the mobility of U(IV) is obviously decreased, which is useful for the immobilization of U(VI) and thereby reduces the toxicity of U(VI) in the environment [75]. The maximum Cr sorption occurred for the pH in the range of 5–6.5 at 180 min which depicts that 8-HQ-GO-Fe_3O_4 reached equilibrium at pH 6.5 and 180 min for the Cr (VI) ion. The phenomenon may be due to the use of the small molecule 8-HQ as a chelating agent in analytical chemistry, owing to its oxygen donor atom and nitrogen donor atom that can form a complex with Cr (VI) [76,77]. Therefore, a contact time of 180 min definitely suggests that equilibrium was achieved. The interaction effect between initial Cr (VI) concentration

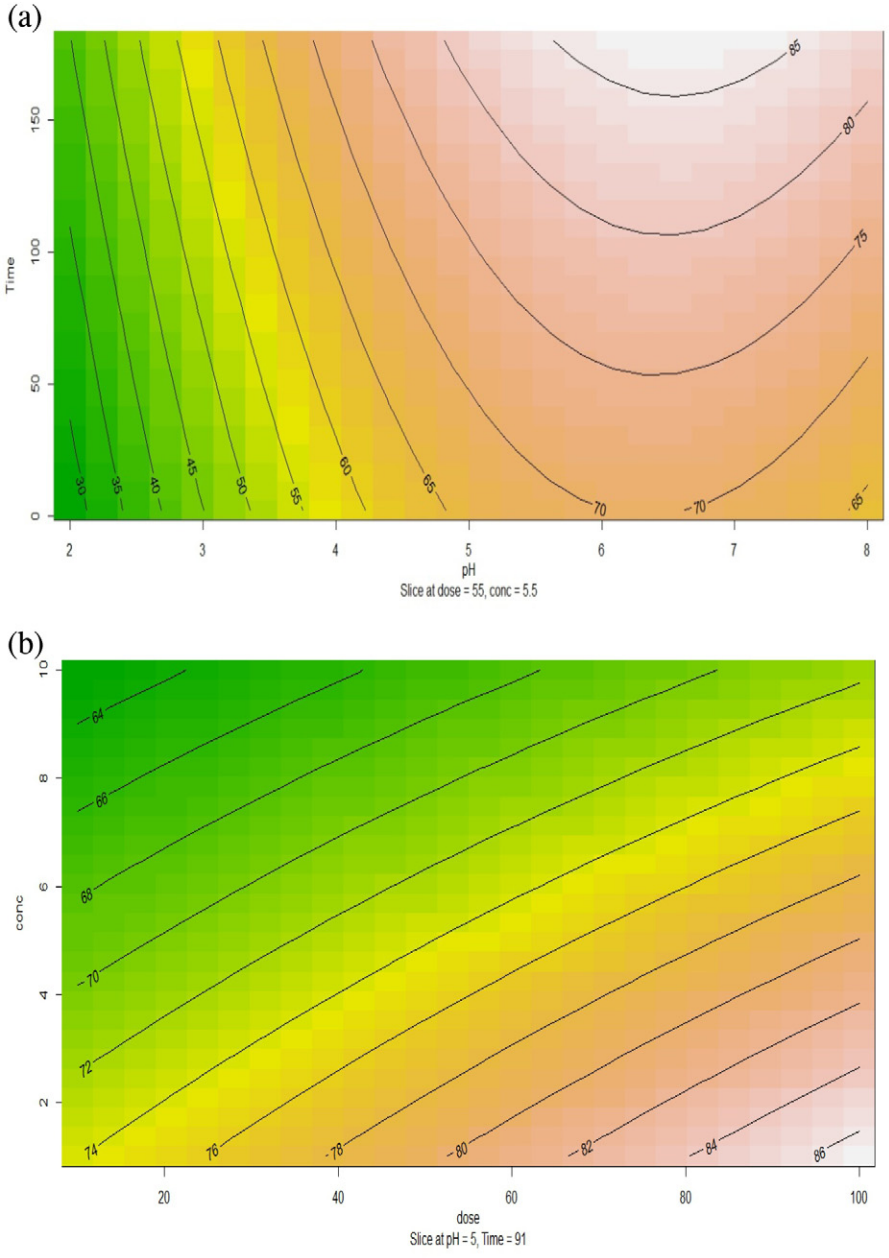

Fig. 8. Contour plot for the effect of pH and time (a) and initial concentration of Cr (VI) and adsorbent dosage (b).

(2–9 mg L^{-1}) and adsorbent dosage (20–100 g L^{-1}) on the adsorption of Cr (VI) ions onto 8-HQ- GO-Fe_3O_4 were monitored at a pH of 5.0 and a time of 91 min and presented in Fig. 8b. The adsorbent dosage has a direct relation to the uptake capacity of an adsorbent. As shown in Fig. 8b, adsorption effectiveness increased with the increase of adsorbent dose from 2 to 9 mg (at a fixed initial Cr (VI) concentration (2 mg L^{-1}), pH 5.0 and 91 min and reached from 74 to 86%) and thereafter remained unchanged. An increase in uptake capacity, with increasing adsorbent dosage, can be attributed to the greater accessibility of the active sites or surface of the sorbent for adsorption, pore diffusion of the Cr (VI) into the bulk of the adsorbent (interior surface) and also the increase of the active and accessible linking sites for the sorbent [25,76,78]. However, further increments in sorbent dose above 100 g L^{-1} did not exhibit improvements in the removal efficiency that can be due to the aggregation of available binding sites [78]. The interaction effect of initial Cr (VI) concentration on adsorbent dosage at pH 5.0 and 91 min was investigated and is presented in Fig. 8b. As indicated in Fig. 8b, in a fixed dose of sorbent (e.g. 2 g L^{-1}) with increasing Cr (VI) concentrations from 2 to 9, the present removal of Cr (VI) decreases from 74 to 64%. For a given mass of the adsorbent, the surface binding sites on the adsorbent are fixed; therefore, the removal percentage of the pollutant may decrease as its initial concentration increases that can be due to the saturation of the binding sites [25,76,78]; however, in some studies, the removal percentage of the pollutant increased for increasing initial pollutant concentrations that shows the internal part of the adsorbent was also used for pollutant sorption [78].

3.6. Isotherm study

An isotherm describes the distribution of adsorbate molecules between the liquid phase and the solid phase at equilibrium and a constant temperature that is an important step for the design of adsorption systems. So, in this study, the relationship between the amount of Cr (VI) ions adsorbed onto 8-HQ-GO-Fe_3O_4 at given experimental conditions in liquid phase was described by isotherm, and equilibrium data were fitted onto the Langmuir, Freundlich and Temkin isotherm models using the correlation coefficient (R^2) [79,80]. Isotherm parameters for the three isotherm models showing an accurate fit of equilibrium data, confirmed by the closeness of the regression values, are presented in Table 7. The Langmuir model assumes the adsorbent surface is covered with a complete monolayer that can caused a limited adsorption capacity, the adsorbent layers are uniform and the adsorption of a molecule to a given site is not dependent on the neighboring sites. The Freundlich isotherm assumes multi-molecular layer adsorption, uneven adsorption of the adsorbate on the adsorbent surface, lack of uniform distribution of energy and a variety of interactions between the adsorbent and the adsorbate. The Temkin isotherm suggests the decrease of the heat of adsorption linearly throughout the adsorption process [67,81,82]. As Table 4 shows, the maximum adsorption capacity increased with an increase in temperature and reached from 10 to 11.9 mg g^{-1}, yet no observed significant difference between different temperatures was observed. Wen study group indicated excellent adsorption capacity toward Cr (VI) (156.94 mg g^{-1}) for the PANI/H-TNB composites [22] In study conducted by Wencai et al. the maximum sorption capacity of Cr(VI) on CNFs in single-metal systems at pH 5.0 and 303 K was calculated as 2.36 by Langmuir equation [21]. The values of the Langmuir constant (b) indicated good affinity between the sorbent and sorbate at all temperatures, as it was observed 1.35, 1.28 and 1.27 (L/mg) values for 288 K, 298 K and 308 K of temperature. Decrease of b values with increasing temperature implies that the sorption process is exothermic. This phenomenon showed the low impact of increased temperatures on the bonding [81]. The essential feature of the Langmuir isotherm can be described by a dimensionless separation factor (R_L) or equilibrium parameter. According to Table 7, the value of R_L was in the range of 0.058–0.061; this indicated that adsorption of Cr (VI) on 8-HQ-GO-Fe_3O_4 is favorable at all temperatures. Moreover, decreasing the solute temperature led to a decrease in the value of the separation factor (R_L) indicating that the adsorption was more favorable. This phenomenon was also confirmed by the Freundlich constant (n), 2.22, 2.17 and 1.35 for temperatures of 288 K, 298 K and 308 K, respectively. Additionally, it was observed that n values are greater than unity for each of the three temperatures indicating chemisorptions of Cr (VI). The greater the value of K_F obtained for 288 K than 308 K, the stronger the adsorption ability of 8-HQ-GO-Fe_3O_4 for higher temperatures will be, and at higher temperatures the heterogeneous adsorption sites played a more important role [83]. The Temkin isotherm is also available for heterogeneous adsorption of the adsorbate on a surface. The high value of the adsorption heat (b_1), shows the fast sorption of the adsorbate at the initial stage. Moreover, the low value of the equilibrium binding constant (k_t) was related to the weak bonding of the adsorbate onto the medium. The order of adsorption heats (b_1) were 5.09, 5.26 and 5.44 for temperatures of 288 K, 298 K and 308 K, respectively. Also the obtained values of k_t for 288 K, 298 K and 308 K temperatures were 0.004, 0.003 and 0.002 (L/g), respectively. Based on the obtained results, the highest adsorption heat (b_1) and the lowest equilibrium binding constant (k_t) were related to the highest temperature rather than other temperatures indicating the highest sorption of chromium at the initial stage and a weak bonding of chromium on 8-HQ- GO-Fe_3O_4, respectively [81–83]. Based on the reported results in Table 7, high correlation coefficients (R^2) were found for the Langmuir model compared with the Freundlich and Temkin models that confirm a reasonable fit to the data, with R^2 of 0.994, 0.998 and 0.994 for 288 K, 298 K and 308 K temperatures, respectively. Also, this implies that 8-HQ-GO-Fe_3O_4 has a monolayer sorption behavior similar to that of the Langmuir model.

Table 7
Adsorption isotherm parameters for adsorption of Cr (VI) on 8-HQ-GO-Fe_3O_4 at different temperatures.

Isotherm model	T			
		288 K	298 K	308 K
Langmuir	q_m (mg g^{-1})	10	10.9	11.9
	b (L/mg)	1.35	1.28	1.27
	R_L	0.058	0.061	0.061
	r^2	0.994	0.998	0.994
Freundlich	K_f ($mg^{1-1/n}/L^{1/n}/g$)	4.89	5.01	5.12
	n	2.22	2.17	1.35
	r^2	0.969	0.971	0.973
Temkin	k_t (L/g)	0.004	0.003	0.002
	b_1	5.09	5.26	5.44
	r^2	0.990	0.992	0.994

3.7. Thermodynamic study

The related results with the thermodynamic parameters such as Ea, ΔH^0, ΔS^0 and ΔG^0 are summarized in Table 8. In the present work, the value of Ea was found to be 1.39 kJ mol^{-1} indicating chemical adsorption rather than physisorption for adsorption of Cr (VI) onto the 8-HQ-GO-Fe_3O_4 adsorbent. The positive value also indicates an endothermic reaction [81]. The value of ΔH^0 for this research was positive, showing that the sorption reaction was endothermic, i.e., the q_e increases with increasing T. The negative or positive standard entropy change

Table 8
Thermodynamic parameters for Cr (VI) adsorption onto 8-HQ- GO-Fe_3O_4.

Studied adsorbent	Enthalpy (ΔH^0) (kJ mol^{-1})	Entropy (ΔS^0) (kJ mol^{-1} K^{-1})	ΔG^0 (kJ mol^{-1})		
			Absolute temperature, T (K)		
			288	298	308
8-HQ-GO-Fe_3O_4	1.36	0.025	−6.07	−6.31	−6.6

(ΔS^0) values imply a decrease or an increase in the randomness at the solid/liquid interface during the sorption process respectively (a decrease or an increase in the degree of freedom of the adsorbed ions). The ΔS^0 value for adsorption of Cr (VI) onto 8-HQ-GO-Fe_3O_4 was positive indicating an increase in the degree of freedom of the adsorbed ions. The positive or negative values of the ΔG^0 indicated that the adsorption process is non-spontaneous and spontaneous, respectively. In addition, ΔG^0 values were negative at all of the temperatures (288–308 K) indicating that the sorption of Cr (VI) was thermodynamically spontaneous and favorable [81–83]. Also the negative value of ΔG^0 increases with increasing temperature showing the endothermic nature of the reaction between adsorbent active sites and Cr (VI) ions [83].

3.8. Kinetic study

The sorption kinetic study in a wastewater treatment is very important, because it determines the mechanism of adsorption (such as chemical reaction, diffusion control and mass transfer) and provides valuable insights into the reaction pathways and mechanism of sorption reaction. Hence, time-concentration profiles of the sorption of Cr (VI) by the 8-HQ-GO-Fe_3O_4 adsorbent was used to study kinetic models, including pseudo-first order, pseudo-second order, Elovich and intra-particle diffusion. The parameters of the kinetic models are presented in Table 9. The pseudo-first order kinetic model describes sorption in solid-liquid systems based on the sorption capacity of solids, and it is assumed that one pollutant molecule is sorbed onto one sorption site on the adsorbent surface. The pseudo-second order kinetic model assumes that the pollutant molecules are sorbed onto sorption sites on the adsorbent surface and the rate limiting step may be a chemical adsorption involving sharing or exchange of electrons between the sorbent and the sorbate. The Elovich kinetic model is based on the chemisorption phenomena that can be used for describing the second-order kinetics, assuming that the actual solid surfaces are energetically heterogeneous [81–84]. As can be seen from Table 9, experimentally observed q_e values for the pseudo-first order and pseudo-second order models were in poor agreement with those calculated and derived from these two models for all Cr (VI) concentrations. For the pseudo-first order model, the decrease of the rate constants (k_1) with increasing initial concentrations of Cr (VI) can be the other reason for the insufficiency of the model to fit the experimental kinetic data for all the initial concentrations examined, although for the pseudo-second order model, increase of the rate constants (k_2) with increasing initial concentrations of Cr (VI) is not necessary. For the Elovich model, predicted q_e values agree well with those obtained experimentally. Furthermore, high predicted R^2 values were obtained for the Elovich model. This agreement is indicative of the applicability of the Elovich model to fit the experimental kinetic data for the present system. This relies on the chemisorption phenomena of Cr (VI) by 8-HQ-GO-Fe_3O_4, assuming that the actual solid surfaces are energetically heterogeneous [83,84]. In order to gain insight into the mechanisms and rate controlling steps affecting the kinetics, the data were tested using the intra-particle diffusion model, which has often been used to investigate the adsorption rate controlling step. According to this model, if the plot of q versus $t^{0.5}$ is straight line, intra-particle diffusion is involved in the adsorption process and it will be the sole rate-limiting step if the plot passes through the origin. Also, according to the intra-particle model, if multi-linear plots involve various steps, then two or more steps influence the adsorption process. Fig. 9 shows the intra-particle diffusion plots for the different concentrations of Cr (VI) adsorption onto 8-HQ-GO-Fe_3O_4. It can be seen that all the plots have the same general feature and are multi-linear, indicating that two steps take place at the initial curved portion (steeper portion) the instantaneous adsorption or external surface adsorption. This portion is followed by a linear portion or a sharper portion where the intra-particle or pore diffusion is rate limiting. The plateau portion of the curve is attributed to the final equilibrium stage where intra-particle diffusion starts to slow down due to extremely low adsorbate

Table 9
Kinetic parameters for Cr (VI) adsorption onto 8-HQ-GO-Fe_3O_4 at different initial concentration.

C_0 mg L^{-1}	Pseudo-first-order				Pseudo-second-order				Elovich				Intra-particle diffusion							
													First line (surface diffusion)				Second line (intraparticle diffusion)			
	q_e, exp. (mg g^{-1})	q_e, cal. (mg g^{-1})	k_1 (min^{-1})	R^2	q_e, cal. (mg g^{-1})	k_2 (g $mg^{-1}min^{-1}$)	h_0 (mg g^{-1} min^{-1})	R^2	q_e, cal. (mg g^{-1})	α (mg g^{-1} min^{-1})	β(g mg^{-1})	R^2	k_d (mg $g^{-1}min^{-1/2}$)	I (mg g^{-1})	R^2		k_d (mg $g^{-1}min^{-1/2}$)	I (mg g^{-1})	R^2	
3	2.76	1.5	0.02	0.93	2.9	0.028	0.23	0.99	2.8	0.95	2.1	0.99	0.68		0.09	0.96	0.04		2.2	0.98
6	5.28	3.7	0.014	0.98	5.9	0.007	0.22	0.98	4.8	1.01	1.08	0.99	1.11		0.06	0.94	0.24		2.3	0.97
9	7.34	6.3	0.014	0.97	8.3	0.003	0.20	0.97	6.7	0.91	0.7	0.98	1.6		−0.55	0.99	0.4		2.5	0.97

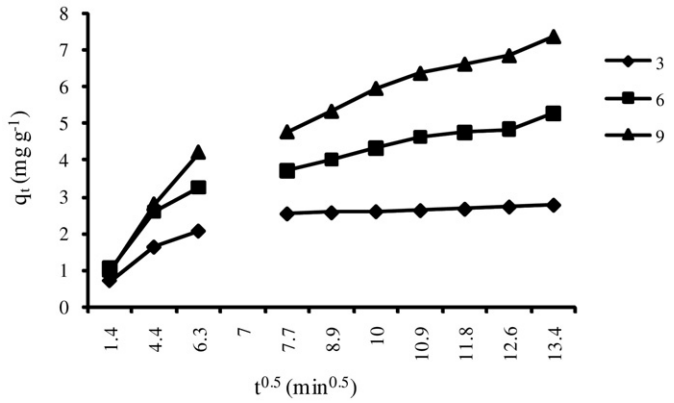

Fig. 9. Intraparticle diffusion model for adsorption of Cr (VI) onto 8-HQ - functionalized GO-Fe_3O_4 nanocomposite.

concentrations left in the solutions. This indicates that the process may be controlled by external surface adsorption and intra-particle diffusion but only one was rate-limiting in any particular time range. Higher values of K_d (indicates rapid transfer) and I (negative value of I indicates no boundary layer effect on the rate of adsorption) for intra-particle diffusion than surface diffusion confirms intra-particle diffusion as the dominant mechanism for the adsorption of Cr (VI) onto8-HQ-GO-Fe_3O_4. Thus, intra-particle diffusion is the dominant mechanism for the adsorption but it is not the sole rate controlling step [84].

4. Conclusions

In the present study, RSM using R software was chosen to evaluate the relationship between input-independent factors (pH, 8-HQ/GO dose, time and Cr (VI) concentration) and one dependent output response (removal efficiency) on Cr (VI) sorption onto 8-HQ- GO-Fe_3O_4. The lower *P*-value (1.33×10^{-15}), higher F-value (240.4), higher R^2 (multiple R-squared: 0.994, adjusted R-squared: 0.989), insignificant lack of fit (0.38) and AIC (48.74) indicate that the reduced full second-order model is highly significant for Cr (VI) removal by 8-HQ- GO-Fe_3O_4 and it also represents the satisfactory adjustment between model and experimental data. The results indicate that the R-squared value of the model is very close to the adjusted R-squared value that expresses a good chance for significant terms to be included in the model; therefore, the quadratic regression related to the reduced full second-order model can be used for prediction and optimization. The terms of x_4, x_2: x_4, x_1^2 showed an antagonistic effect on the model, while other terms had a synergistic effect on the response prediction by the model. The maximum removal efficiency was estimated as 95.77% (to involve all parameters simultaneously) using regression coefficients obtained from the model and Solver "Add-ins". The predicted optimal conditions by the Solver method in the maximum removal efficiency, were achieved at initial Cr (VI) concentration 1 mg L^{-1}, adsorbent dose 98.4 (g L^{-1}), time 178.4 (min) and pH 6.55 that was very close to the stationary point in original units. The relationship between the amount of Cr (VI) ions adsorbed onto 8-HQ-GO-Fe_3O_4 under the given experimental conditions in liquid phase was described by isotherm, and equilibrium data were fitted onto Langmuir, Freundlich and Temkin isotherm models using the correlation coefficient (R^2). Based on the reported results, high correlation coefficients (R^2) were found for the Langmuir model compared with the Freundlich and Temkin models that confirm the reasonable fit to the data, with R^2 of 0.994, 0.998 and 0.994 for 288 K, 298 K and 308 K temperatures, respectively. Also, this implies that the 8-HQ-GO-Fe_3O_4 has monolayer sorption behavior similar to that of the Langmuir model. The maximum adsorption capacity increased with an increase in temperature and reached 11.9 mg g^{-1} 308 K. The thermodynamic data with $\Delta H^0 > 0$, $\Delta S^0 > 0$ and $\Delta G^0 < 0$ (at all of the temperatures (288–308 K)) revealed an endothermic reaction, an increase in the degree of freedom of the adsorbed ions and spontaneous sorption in the nature of adsorption process. Also the Ea value found to be 1.39 kJ mol^{-1} was indicative of chemical sorption for Cr (VI). Time-concentration profiles of the sorption of Cr (VI) by 8-HQ-GO-Fe_3O_4 adsorbent was used to study the kinetic models, including pseudo-first order, pseudo-second order, Elovich and intra-particle diffusion. For the Elovich model, predicted q_e values agree well with those obtained experimentally. Additionally, high predicted R^2 values were obtained for the Elovich model and this agreement indicates the applicability of the Elovich model to fit the experimental kinetic data for the present system. This relies on the chemisorption phenomena of Cr (VI) by 8-HQ-GO-Fe_3O_4, assuming that the actual solid surfaces are energetically heterogeneous. Also it was observed that intra-particle diffusion is the dominant mechanism for the adsorption but it is not the sole rate controlling step.

Acknowledgement

This study is related to the project NO. 1395/66080 from Student Research Committee, Shahid Beheshti University of Medical Sciences, Tehran, Iran. We also appreciate the "Student Research Committee" and "Research & Technology Chancellor" in Shahid Beheshti University of Medical Sciences for their financial support of this study.

References

[1] L. Alidokht, A. Khataee, A. Reyhanitabar, S. Oustan, Desalination 270 (2011) 105–110.
[2] D. Chauhan, N. Sankararamakrishnan, J. Hazard. Mater. 185 (2011) 55–62.
[3] Y. Hou, H. Liu, X. Zhao, J. Qu, J.P. Chen, J. Colloid Interface Sci. 385 (2012) 147–153.
[4] M.A. Rahman, M. Muneer, Desalination 181 (2005) 161–172.
[5] P. Wu, S. Li, L. Ju, N. Zhu, J. Wu, P. Li, Z. Dang, J. Hazard. Mater. 219 (2012) 283–288.
[6] H. Zhang, Y. Tang, D. Cai, X. Liu, X. Wang, Q. Huang, Z. Yu, J. Hazard. Mater. 181 (2010) 801–808.
[7] Y.-X. Liu, D.-X. Yuan, J.-M. Yan, Q.-L. Li, T. Ouyang, J. Hazard. Mater. 186 (2011) 473–480.
[8] B. Wielinga, M.M. Mizuba, C.M. Hansel, S. Fendorf, Environ. Sci. Technol. 35 (2001) 522–527.
[9] L. Calder, Adv. Environ. Sci. Technol. 20 (1988) 215–229.
[10] M. Chiha, M.H. Samar, O. Hamdaoui, Desalination 194 (2006) 69–80.
[11] H. Daraei, A. Mittal, J. Mittal, H. Kamali, Desalin. Water Treat. 52 (2014) 1307–1315.
[12] E.M. Kalhori, K. Yetilmezsoy, N. Uygur, M. Zarrabi, R.M.A. Shmeis, Appl. Surf. Sci. 287 (2013) 428–442.
[13] M.A. Salam, G. Al-Zhrani, S.A. Kosa, J. Ind. Eng. Chem. 20 (2014) 572–580.
[14] M.A. Salam, G. Al-Zhrani, S.A. Kosa, C. R. Chim. 15 (2012) 398–408.
[15] T. Phetla, F. Ntuli, E. Muzenda, J. Ind. Eng. Chem. 18 (2012) 1171–1177.
[16] M. Sarkhosh, Z. Atafar, E. Ahmadi, S. Nazari, Y. Fakhri, S. Rezaei, S.M. Mohseni, M.H. Saghi, B. Baziar, Int. J. Curr. Microbiol. App. Sci. 5 (2016) 615–625.
[17] V. Prigione, M. Zerlottin, D. Refosco, V. Tigini, A. Anastasi, G.C. Varese, Bioresour. Technol. 100 (2009) 2770–2776.
[18] A. Sarı, Ö.D. Uluozlü, M. Tüzen, Chem. Eng. J. 167 (2011) 155–161.
[19] R.-S. Juang, S.-H. Lin, L.-C. Peng, Chem. Eng. J. 161 (2010) 19–26.
[20] F. Fu, L. Xie, B. Tang, Q. Wang, S. Jiang, Chem. Eng. J. 189 (2012) 283–287.
[21] W. Cheng, C. Ding, X. Wang, Z. Wu, Y. Sun, S. Yu, T. Hayat, X. Wang, Chem. Eng. J. 293 (2016) 311–318.
[22] T. Wen, Q. Fan, X. Tan, Y. Chen, C. Chen, A. Xu, X. Wang, Polym. Chem. 7 (2016) 785–794.
[23] M.M. Areco, S. Hanela, J. Duran, M. dos Santos Afonso, J. Hazard. Mater. 213 (2012) 123–132.
[24] U. Maheshwari, B. Mathesan, S. Gupta, Process. Saf. Environ. Prot. 98 (2015) 198–210.
[25] W. Guo, X. Meng, Y. Liu, L. Ni, Z. Hu, R. Chen, M. Meng, Y. Wang, J. Han, M. Luo, J. Ind. Eng. Chem. 21 (2015) 340–349.
[26] Y.-S. Shen, S.-L. Wang, Y.-M. Tzou, Y.-Y. Yan, W.-H. Kuan, Bioresour. Technol. 104 (2012) 165–172.
[27] Q. Yuan, N. Li, Y. Chi, W. Geng, W. Yan, Y. Zhao, X. Li, B. Dong, J. Hazard. Mater. 254 (2013) 157–165.
[28] M. Xu, W. Linghu, J. Hu, G. Jiang, J. Sheng, J. Phys. Chem. Solids 98 (2016) 100–106.
[29] Y. Li, G. Sheng, J. Sheng, J. Mol. Liq. 199 (2014) 474–480.
[30] J.D. Fowler, M.J. Allen, V.C. Tung, Y. Yang, R.B. Kaner, B.H. Weiller, ACS Nano 3 (2009) 301–306.
[31] Z.-J. Fan, W. Kai, J. Yan, T. Wei, L.-J. Zhi, J. Feng, Y.-m. Ren, L.-P. Song, F. Wei, ACS Nano 5 (2010) 191–198.
[32] M. Seredych, T.J. Bandosz, Carbon 45 (2007) 2130–2132.
[33] Y. Matsuo, Y. Nishino, T. Fukutsuka, Y. Sugie, Carbon 46 (2008) 1162–1163.
[34] V. Chandra, K.S. Kim, Chem. Commun. 47 (2011) 3942–3944.
[35] S.-T. Yang, Y. Chang, H. Wang, G. Liu, S. Chen, Y. Wang, Y. Liu, A. Cao, J. Colloid Interface Sci. 351 (2010) 122–127.

[36] S.-T. Yang, S. Chen, Y. Chang, A. Cao, Y. Liu, H. Wang, J. Colloid Interface Sci. 359 (2011) 24–29.
[37] Y. Zou, X. Wang, Z. Chen, W. Yao, Y. Ai, Y. Liu, T. Hayat, A. Alsaedi, N.S. Alharbi, X. Wang, Environ. Pollut. 219 (2016) 107–117.
[38] X. Ren, Q. Wu, H. Xu, D. Shao, X. Tan, W. Shi, C. Chen, J. Li, Z. Chai, T. Hayat, Environ. Sci. Technol. 50 (2016) 9361–9369.
[39] Y. Zou, X. Wang, Y. Ai, Y. Liu, J. Li, Y. Ji, X. Wang, Environ. Sci. Technol. 50 (2016) 3658–3667.
[40] X. Kong, R. Gao, X. He, L. Chen, Y. Zhang, J. Chromatogr. A 1245 (2012) 8–16.
[41] S. Xuan, F. Wang, Y.-X.J. Wang, C.Y. Jimmy, K.C.-F. Leung, J. Mater. Chem. 20 (2010) 5086–5094.
[42] L. Shao, Z. Ren, G. Zhang, L. Chen, Mater. Chem. Phys. 135 (2012) 16–24.
[43] M. Baikousi, A.B. Bourlinos, A. Douvalis, T. Bakas, D.F. Anagnostopoulos, J.I. Tuček, K.R. Šafářová, R. Zboril, M.A. Karakassides, Langmuir 28 (2012) 3918–3930.
[44] Z. Wu, W. Li, P.A. Webley, D. Zhao, Adv. Mater. 24 (2012) 485–491.
[45] C. Chen, J. Hu, D. Shao, J. Li, X. Wang, J. Hazard. Mater. 164 (2009) 923–928.
[46] G.G. Wildgoose, C.E. Banks, H.C. Leventis, R.G. Compton, Microchim. Acta 152 (2006) 187–214.
[47] J.S. Carletto, K.C.D.P. Roux, H.F. Maltez, E. Martendal, E. Carasek, J. Hazard. Mater. 157 (2008) 88–93.
[48] S.A. Kosa, G. Al-Zhrani, M.A. Salam, Chem. Eng. J. 181 (2012) 159–168.
[49] T.E. Milja, K.P. Prathish, T.P. Rao, J. Hazard. Mater. 188 (2011) 384–390.
[50] M. Hebrant, M. Rose-Helene, J.-P. Joly, A. Walcarius, Colloids Surf. A Physicochem. Eng. Asp. 380 (2011) 261–269.
[51] Y. Li, B. Gao, X. Fang, J. Chem. Technol. Biotechnol. 88 (2013) 1459–1467.
[52] F. Shakerian, S. Dadfarnia, A.M.H. Shabani, Food Chem. 134 (2012) 488–493.
[53] M. Khajeh, Biol. Trace Elem. Res. 145 (2012) 118–125.
[54] M. Khayet, A. Zahrim, N. Hilal, Chem. Eng. J. 167 (2011) 77–83.
[55] J.-P. Wang, Y.-Z. Chen, Y. Wang, S.-J. Yuan, H.-Q. Yu, Water Res. 45 (2011) 5633–5640.
[56] J.A. Wass, Biotech Software & Internet Report: The Computer Software Journal for Scientist, 1, 2000 88–95.
[57] B. Jones, J. Sall, Wiley Interdisciplinary Reviews: Computational Statistics, 3, 2011 188–194.
[58] C. Statgraphics, StatPoint Technologies Inc, Warrenton, 2009.
[59] G.E. Box, K. Wilson, On the Experimental Attainment of Optimum Conditions, Springer, 1992 270–310.
[60] R. Subramaniam, S.K. Ponnusamy, Water Resources and Industry, 11, 2015 64–70.
[61] R.V. Lenth, J. Stat. Softw. 32 (2009) 1–17.
[62] A.M. Bandpei, S.M. Mohseni, A. Sheikhmohammadi, M. Sardar, M. Sarkhosh, M. Almasian, M. Avazpour, Z. Mosallanejad, Z. Atafar, S. Nazari, Korean J. Chem. Eng. 2016 1–8.
[63] W.S. Hummers Jr., R.E. Offeman, J. Am. Chem. Soc. 80 (1958) 1339.
[64] Q. Chang, S. Song, Y. Wang, J. Li, J. Ma, Anal. Methods 4 (2012) 1110–1116.
[65] D. Li, M.B. Mueller, S. Gilje, R.B. Kaner, G.G. Wallace, Nat. Nanotechnol. 3 (2008) 101–105.
[66] R. Kumar, (2011).
[67] A.S. Mohammadi, M. Sardar, M. Almasian, Environ. Eng. Manag. J. 15 (2016).
[68] G. Fereshteh, M. Hosein, M. Geoffrey, J. Appl. Sci. 6 (2006) 2705–2714.
[69] H. Aslani, R. Nabizadeh, S. Nasseri, A. Mesdaghinia, M. Alimohammadi, A.H. Mahvi, N. Rastkari, S. Nazmara, Desalin. Water Treat. (2016) 1–12.
[70] D. Podstawczyk, A. Witek-Krowiak, A. Dawiec, A. Bhatnagar, Ecol. Eng. 83 (2015) 364–379.
[71] P. Sudamalla, P. Saravanan, M. Matheswaran, Environ. Res. 22 (2012) 1–7.
[72] X. Wang, Q. Fan, S. Yu, Z. Chen, Y. Ai, Y. Sun, A. Hobiny, A. Alsaedi, X. Wang, Chem. Eng. J. 287 (2016) 448–455.
[73] Y. Sun, X. Wang, C. Ding, W. Cheng, C. Chen, T. Hayat, A. Alsaedi, J. Hu, X. Wang, ACS Sustain. Chem. Eng. 4 (2016) 4608–4616.
[74] M.R. Samani, S.M. Borghei, A. Olad, M.J. Chaichi, J. Hazard. Mater. 184 (2010) 248–254.
[75] X. Wang, S. Yu, J. Jin, H. Wang, N.S. Alharbi, A. Alsaedi, T. Hayat, X. Wang, Sci. Bull. 61 (2016) 1583–1593.
[76] K. Naddafi, N. Rastkari, R. Nabizadeh, R. Saeedi, M. Gholami, M. Sarkhosh, Desalin. Water Treat. 57 (2016) 5789–5799.
[77] Y. Zhang, Y. Lam, W. Tan, J. Colloid Interface Sci. 285 (2005) 74–79.
[78] A. Mohseni-Bandpi, T.J. Al-Musawi, E. Ghahramani, M. Zarrabi, S. Mohebi, S.A. Vahed, J. Mol. Liq. 218 (2016) 615–624.
[79] C.-S. Jeon, K. Baek, J.-K. Park, Y.-K. Oh, S.-D. Lee, J. Hazard. Mater. 163 (2009) 804–808.
[80] H. Godini, F. Hashemi, L. Mansuri, M. Sardar, G. Hassani, S. Mohseni, A. Alinejad, S. Golmohammadi, A.S. Mohammadi, J. Water Reuse Desalin. 6 (2016) 544–552.
[81] H. Liu, W. Liu, J. Zhang, C. Zhang, L. Ren, Y. Li, J. Hazard. Mater. 185 (2011) 1528–1535.
[82] M. Ncibi, S. Altenor, M. Seffen, F. Brouers, S. Gaspard, Chem. Eng. J. 145 (2008) 196–202.
[83] G. Moussavi, R. Khosravi, J. Hazard. Mater. 183 (2010) 724–730.
[84] K. Vilcinskas, J. Zlopasa, K. Jansen, F.M. Mulder, S.J. Picken, G.J. Koper, Macromol. Mater. Eng. 301 (2016) 1049–1063.